Check for updates

Earth's Future

RESEARCH ARTICLE
10.1029/2024EF005151

Soil Drying Intensification Increases the Connection Between Dry and Hot Extremes in a Changing Climate

Yamin Qing[1] **and Shuo Wang**[1,2]

[1]Department of Land Surveying and Geo-Informatics, The Hong Kong Polytechnic University, Hong Kong, China, [2]Research Institute for Land and Space, The Hong Kong Polytechnic University, Hong Kong, China

Key Points:

- Probability of hot extremes following rapidly evolving dry extremes is nearly twice as high as those following slowly evolving dry extremes in the northern mid-high latitudes (≥30°N)
- Higher probability of rapidly evolving dry extremes followed by hot extremes is linked to increased atmospheric aridity and enhanced radiation
- Regions with stronger coupling of land–atmosphere witness a higher probability of hot extremes following rapidly evolving dry extremes

Supporting Information:

Supporting Information may be found in the online version of this article.

Correspondence to:

S. Wang,
shuo.s.wang@polyu.edu.hk

Citation:

Qing, Y., & Wang, S. (2025). Soil drying intensification increases the connection between dry and hot extremes in a changing climate. *Earth's Future*, *13*, e2024EF005151. https://doi.org/10.1029/2024EF005151

Received 2 AUG 2024
Accepted 11 APR 2025

Author Contributions:

Conceptualization: Shuo Wang
Data curation: Yamin Qing
Formal analysis: Yamin Qing
Funding acquisition: Shuo Wang
Investigation: Shuo Wang
Methodology: Yamin Qing, Shuo Wang
Project administration: Shuo Wang
Resources: Shuo Wang
Software: Yamin Qing
Supervision: Shuo Wang
Validation: Yamin Qing
Visualization: Yamin Qing
Writing – original draft: Yamin Qing
Writing – review & editing: Yamin Qing, Shuo Wang

© 2025. The Author(s).
This is an open access article under the terms of the Creative Commons Attribution License, which permits use, distribution and reproduction in any medium, provided the original work is properly cited.

Abstract Global warming intensifies dry and hot extremes as well as their cascade occurrences, leading to devastating impacts on the environment, economy, and society. However, the linkages between dry and hot extremes remain poorly understood. Here, we examine the soil drying characteristics prior to the occurrence of hot extremes to better understand the dynamic relationship between dry and hot extremes. We find that rapidly evolving dry extremes are more likely (43.22%–44.90%) to be followed by hot extremes compared to slowly evolving ones (31.99%–32.78%), with large disparities observed in the northern mid-high latitudes (≥30°N). This higher probability is associated with elevated vapor pressure deficit and increased radiation, coupled with reduced precipitation. We identify the significant role of land–atmosphere coupling in linking rapid soil dryness and hot extremes. Our findings underscore the increased risk of hot extremes following rapid soil dryness and provide insights into preparedness and adaptation strategies for cascading dry and hot hazards.

Plain Language Summary Despite numerous studies on compound dry and hot extremes (i.e., cascading occurrences of dry and hot extremes) over the past decade, focusing on their spatiotemporal variations and physical mechanisms, the linkages between cascading dry and hot extremes remain largely unexplored. In this study, we investigate the relationship between soil drying intensification during dry extremes and subsequent hot extremes based on observational data sets and model simulations. We find that rapidly evolving dry extremes tend to be followed by more hot extremes in the northern mid-high latitudes (≥30°N). This spatial disparity is associated with elevated vapor pressure deficit, increased radiation, and higher potential evapotranspiration, coupled with reduced precipitation. Furthermore, regions with stronger soil moisture–maximum temperature coupling exhibit a higher probability of rapidly evolving dry and subsequent hot extremes. Additionally, the cascades of rapidly evolving dryness and hot extremes under the highest scenarios (SSP5-8.5) are projected to increase nearly tenfold by the end of the 21st century, indicating a greater risk of cascading hazards involving dry and hot extremes under a warming climate. This study highlights that dry extremes with higher soil drying intensification are more likely to be followed by the occurrence of extreme hot weather, particularly in the northern mid-high latitudes, leading to cascading dry and hot extremes.

1. Introduction

In recent decades, the occurrence of dry and hot extremes has increased significantly, as documented by various studies (Alizadeh et al., 2020; Bevacqua et al., 2022; Feng et al., 2020; Mukherjee & Mishra, 2021; Tripathy et al., 2023; Yin et al., 2023). These events have garnered considerable attention due to their escalating impacts, causing widespread destruction across societal, environmental, and economic domains (Graham et al., 2024; Raymond et al., 2020; Yin et al., 2023; Zeighami et al., 2023). For instance, a devastating dry and hot extreme hit Europe in 2003, resulting in the tragic loss of over 70,000 lives (Robine et al., 2008) and an estimated total economic loss of €15 billion (European Environment Agency, 2023). Similarly, the 2012 summer dry and hot event in the central U.S. led to massive economic losses of approximately $30 billion (Rippey, 2015). Furthermore, these extremes can trigger other natural disasters, such as wildfires and dust storms, leading to further unpredictable losses (Park Williams et al., 2013; Schubert et al., 2004; Yoon et al., 2015). To mitigate these impacts, it is crucial to gain a deeper understanding of the dynamic interactions between dry and hot extremes, enabling more accurate prediction and early warning systems.

Compound dry and hot events result from complex interactions among various physical processes across multiple spatial and temporal scales (Mukherjee et al., 2020; Mukherjee & Mishra, 2021). Previous studies on compound dry and hot events have focused on synoptic circulation patterns that initiate these interactions, as

23284277, 2025, 5, Downloaded from https://agupubs.onlinelibrary.wiley.com/doi/10.1029/2024EF005151 by HONG KONG POLYTECHNIC UNIVERSITY HU NG HOM, Wiley Online Library on [29/09/2025]. See the Terms and Conditions (https://onlinelibrary.wiley.com/terms-and-conditions) on Wiley Online Library for rules of use; OA articles are governed by the applicable Creative Commons License

well as self-intensifying land−atmosphere processes that drive feedback mechanisms between dry and hot events (Chiang et al., 2018; Kang et al., 2022; Maraun et al., 2025; Miralles et al., 2019; Mukherjee et al., 2023; Wang et al., 2024; Wu et al., 2021). Additionally, some studies have highlighted the critical role of soil moisture in the occurrence of compound dry and hot extremes (Alizadeh et al., 2020; Zhou et al., 2021). Soil desiccation leads to a reduction in evaporative cooling and an increase in sensible heat flux between the surface and atmosphere, thereby raising surface temperatures, potentially triggering an extreme hot event or amplifying its magnitude (Fischer et al., 2007; Miralles et al., 2014; Seneviratne et al., 2006; Vogel et al., 2017). Although changes in key climate factors and soil moisture, driven by large-scale climatic processes and/or local weather systems, have been investigated to understand their role in linking dry and hot extremes (Bevacqua et al., 2022; Hao et al., 2022; Mukherjee et al., 2023; Tian et al., 2024; Zhang et al., 2022), the impact of soil drying rate—that is, the speed at which dry extremes develop—on subsequent hot extremes is not well understood. Furthermore, gaining insight into how rapidly drying soils contribute to the onset and amplification of hot extremes can enhance our ability to predict these events. The intensification of soil drying could also serve as an early warning indicator for the occurrence of subsequent hot extremes.

According to the 6th Assessment Report (AR6) from the Intergovernmental Panel on Climate Change (IPCC), there is a high confidence that the cascading occurrence of dry and hot extremes has become more frequent, and the increasing trend will continue with higher warming levels (Seneviratne et al., 2021). This study will complement the IPCC report by focusing on the detection and attribution of cascading dry and hot extremes. To mitigate the hazards of cascading dry and hot extremes, such as the drought–heat event that occurred in June of 2021 in the Southwest United States (Osman et al., 2022), and the record-breaking heatwave in June 2021 following a devastating drought in the Western United States (Liberto, 2021), it is crucial to understand the potential linkages between dry and hot extremes. Therefore, we specifically investigate how rapidly evolving dry extremes contribute to the onset of hot extremes, emphasizing the role of soil moisture deficits in amplifying the occurrence and magnitude of these hot extremes based on multiple reanalyses. The study will enhance the understanding of the dynamic connection between dry and hot extremes, providing insights into preparedness and adaptation strategies for cascading dry and hot hazards.

2. Methods

2.1. Data

Hourly soil moisture (SM) data were obtained from the European Center for Medium-Range Weather Forecasts (ERA5) and the Modern-Era Retrospective Analysis for Research and Applications, version 2 (MERRA-2). The ERA5 and MERRA-2 SM data sets are observationally constrained and have been widely used to analyze global and regional SM changes. Here, we used the 0–100 cm SM to approximate root-zone SM. The MERRA-2 SM data set includes two layers (0–5 cm and 10–100 cm); therefore, root-zone SM at depths of 0–100 cm was obtained using the depth-weighted averaging method. The ERA5 data set provides estimates of root-zone SM at depths of 0–7 cm, 7–28 cm, and 28–100 cm. These values were vertically interpolated to a depth of 0–100 cm using depth-weighted averaging, as shown in Equation 1. For surface SM, the first layer of SM was selected. Hourly SM, 2 m temperature (T), 2 m dewpoint temperature (T), precipitation (Pre), and surface net solar radiation (Rn) data from both data sets were uniformly aggregated to a spatial resolution of 0.5° × 0.5° using the bilinear interpolation method. The daily SM, 2 m T, 2 m dewpoint T, VPD, and Rn were calculated as the average values recorded over a 24-hr period. The daily maximum temperature (T_{max}) was calculated as the highest value recorded over a 24-hr period. The daily precipitation was calculated as the total amount recorded over a 24-hr period. Specifically, daily VPD was calculated as the difference between saturated water vapor pressure, determined by daily 2 m T, and actual water vapor pressure, determined by daily 2 m dewpoint T. All data were then aggregated to a pentad (5-day) temporal resolution for 1980–2020.

$$SM_{RZ} = (SM_1 * 7 + SM_2 * 21 + SM_3 * 72)/100 \quad (1)$$

where SM_{RZ} is root-zone SM at depth of 0–100 cm, SM_1, SM_2, and SM_3 is SM at depth of 0–7 cm, 7–28 cm, and 28–100 cm.

10.1029/2024EF005151

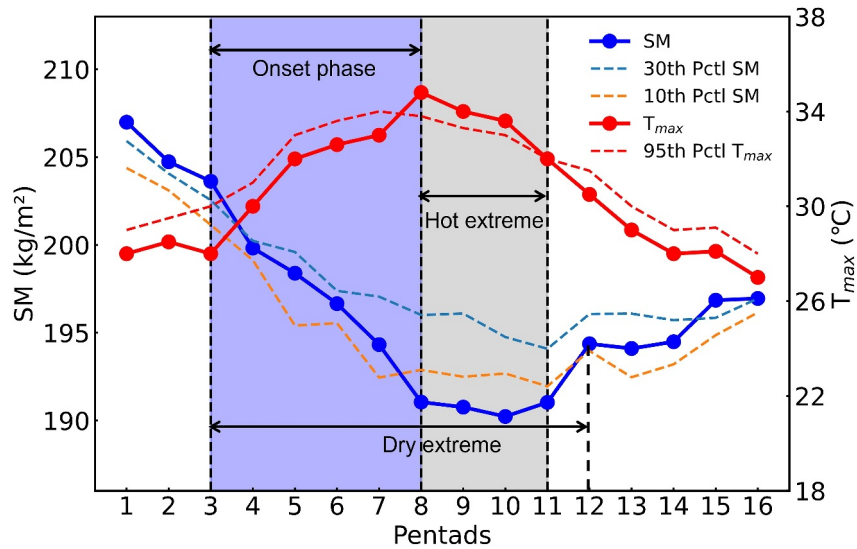

Figure 1. Schematic representation of the method used to identify the RDH. The blue solid line represents the 5-day mean SM changes during the rapidly evolving dry extreme event on a grid point: SM decreases from above the 30th percentile to below the 10th percentile with an average decline rate of no less than the 10th percentile for each pentad during the onset phase. The orange and blue dashed lines represent the 10th and 30th percentiles of SM, respectively, at a particular time of the year during the period of 2000–2020. The purple shaded area represents the onset phase of dry extremes. The red solid line represents the 5-day mean maximum temperature (T_{max}) changes during the occurrence of a hot extreme event on a grid point: T_{max} increases from below the 95th percentile to over the 95th percentile after the onset phase of a dry extreme. The red dashed lines represent the 95th percentile of T_{max} at a particular time of the year during the period of 2000–2020. The gray shaded area represents a hot extreme event.

2.2. Definition of Dry and Hot Extremes

In this study, the definitions of rapidly and slowly evolving dry extremes follow a systematic approach. First, the onset phase of dry extremes is identified as the period during which SM decreases from above the 30th percentile to below the 10th percentile. The choice of the 10th percentile ensures that the dry extremes are sufficiently severe. Although a decline from the 40th percentile to below the 20th percentile has also been used in the literature (Ford & Labosier, 2017; Qing et al., 2022; Yuan et al., 2023), the 10th percentile is selected here to capture more pronounced drought conditions. The selection of the 40th and 20th percentiles has also been tested (Figure S1 in Supporting Information S1). Next, the drying rate is assessed: if this decline occurs within six pentads (30 days) with an average SM decline rate greater than 5% in percentile, the event is classified as a rapidly evolving dry extreme (Figure 1) (Qing et al., 2022); otherwise, it is classified as a slowly evolving dry extreme. To identify hot extremes, the maximum temperature (T_{max}) must exceed the 95th percentile of the long-term climatology for each pentad (Figure 1) (Fischer & Schär, 2010; Perkins & Alexander, 2013; You et al., 2023). Finally, rapidly evolving dry extremes followed by hot extremes (RDH) are defined as cases where a hot extreme occurs within two pentads (10 days) after the onset of a rapidly evolving dry extreme, while slowly evolving dry extremes followed by hot extremes (SDH) occur when a hot extreme follows a slowly evolving dry extreme within the same time frame.

The soil drying rate is defined as the SM decline between adjacent pentads (i.e., the difference between the current and next-pentad SM). To assess the relationship between different soil drying rates and subsequent T_{max}, we divide the SM decline between adjacent pentads into six categories: 0–5th, 5–10th, 10–15th, 15–20th, 20–25th, and 25–30th percentiles. Specifically, we first compute the percentile values for raw SM across all pentads based on their ranking within the data set. Next, the SM decline between adjacent pentads is calculated in percentile space by subtracting the percentile value of the next pentad from that of the current pentad. These SM percentile declines are then ranked and classified into six categories: 0–5th, 5–10th, 10–15th, 15–20th, 20–25th, and 25–30th percentiles. Since the sample size for declines beyond the 30th percentile is limited, these cases are incorporated into the 25–30th percentile category to ensure statistical robustness.

23284277, 2025, 5, Downloaded from https://agupubs.onlinelibrary.wiley.com/doi/10.1029/2024EF005151 by HONG KONG POLYTECHNIC UNIVERSITY HU NG HOM, Wiley Online Library on [29/09/2025]. See the Terms and Conditions (https://onlinelibrary.wiley.com/terms-and-conditions) on Wiley Online Library for rules of use; OA articles are governed by the applicable Creative Commons License

2.3. The Two-Sample Kolmogorov–Smirnov (K-S) Test

The two-sample Kolmogorov-Smirnov (K-S) test (Kolmogorov, 1933) was selected to compare the distributions of RDH and SDH. Unlike parametric tests that focus only on differences in mean or variance, the K-S test evaluates the entire distribution function, making it particularly useful for detecting differences in shape, spread, and central tendency between RDH and SDH. To apply the two-sample K-S test, the empirical cumulative distribution functions of RDH and SDH were first computed. A p-value was then obtained to assess the statistical significance of the difference. The test was conducted using the ks_2samp function from the SciPy library in Python. If the p-value was below 0.05, the null hypothesis—stating that RDH and SDH originate from the same distribution—was rejected, indicating a significant difference between the two distributions. Otherwise, no strong evidence was found to suggest a difference in their distributions.

2.4. Modeling the Dependence Structure Between SM and T_{max} Using Bivariate Copulas

To characterize the dependence between SM and T_{max}, we employed bivariate copulas, a widely used statistical tool for modeling relationships between dependent variables (AghaKouchak et al., 2014; Zscheischler & Seneviratne, 2017). The joint probability distribution of SM and T_{max} is expressed as:

$$F_{\mathrm{SM},T_{\max}}(x,y) = P(\mathrm{SM} \le x, T_{\max} \le y) \tag{2}$$

And the marginal cumulative distribution functions are defined as $F_{\mathrm{SM}}(x) = P(\mathrm{SM} \le x)$ and $F_{T_{\max}}(y) = P(T_{\max} \le y)$. We use a bivariate copula C to describe the joint probability distribution of SM and T_{max} as:

$$F_{\mathrm{SM},T_{\max}}(x,y) = C[F_{\mathrm{SM}}(x), F_{T_{\max}}(y)] = C(u,v) \tag{3}$$

The functions $F_{\mathrm{SM}}(x)$ and $F_{T_{\max}}(y)$ are transformed into two uniformly distributed random variables, u and v, which range from 0 to 1 (i.e., the normalized ranks of SM and T_{max}). Given that compound dry and hot extremes are defined as events where SM falls below its 10th percentile and T_{max} exceeds its 90th percentile, the joint probability of such an event is expressed as:

$$P(u < 0.1 \cap v > 0.9) = P(u < 0.1) - P(u < 0.1 \cap v \le 0.9) = 0.1 - C(0.1, 0.9) \tag{4}$$

To model the joint probability distribution, we considered commonly used copula families, including Gaussian, Student's t, Clayton, Gumbel, and Frank copulas. The optimal copula model at each grid point was selected based on the Bayesian Information Criterion (BIC). All copula analyses were performed using the VineCopula package in R.

To quantify the impact of SM on subsequent hot extremes, we computed the Probability Modification Factor (PMF), define as:

$$\mathrm{PMF} = \frac{P_{\mathrm{joint}}^{\mathrm{copula}}}{P_{\mathrm{joint}}^{\mathrm{independent}}} \tag{5}$$

where $P_{\mathrm{joint}}^{\mathrm{copula}}$ represents the joint probability derived from the best-fitting copula model, and $P_{\mathrm{joint}}^{\mathrm{independent}}$ represents the joint probability assuming independent distributions, obtained using the independent copula. The independent copula serves as a baseline to assess how much the actual dependence deviates from statistical independence. For example, we derive the joint probability of independent distributions from the independent copula:

$$P = 0.1 - C(0.1, 0.9) = 0.1 - 0.1 \times 0.9 = 0.01 \tag{6}$$

A PMF of 1 indicates that dry and hot extremes occur independently, while a PMF greater than 1 suggests an increased joint probability due to the dependence between SM and T_{max}. By evaluating the PMF across different regions and conditions, we quantified the extent to which the probability of hot extremes is amplified following dry conditions, relative to an independent occurrence assumption.

23284277, 2025, 5, Downloaded from https://agupubs.onlinelibrary.wiley.com/doi/10.1029/2024EF005151 by HONG KONG POLYTECHNIC UNIVERSITY HU NG HOM, Wiley Online Library on [29/09/2025]. See the Terms and Conditions (https://onlinelibrary.wiley.com/terms-and-conditions) on Wiley Online Library for rules of use; OA articles are governed by the applicable Creative Commons License

10.1029/2024EF005151

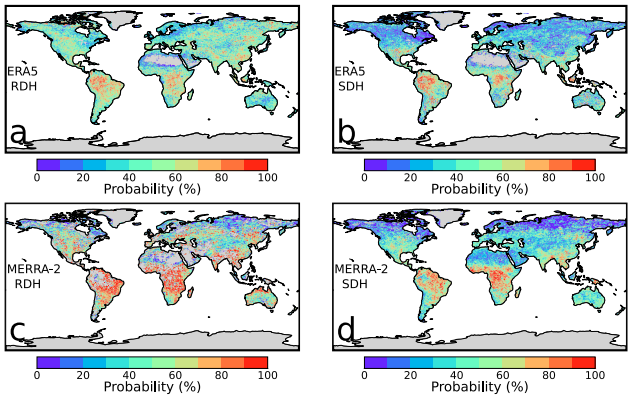

Figure 2. Comparison between the probabilities of RDH and SDH. (a, c) Spatial pattern of the probability of RDH during the period of 1980–2020 based on the ERA5 and MERRA-2 data sets. (b, d) Spatial pattern of the probability of SDH during the period of 1980–2020 based on the ERA5 and MERRA-2 data sets.

3. Results

3.1. Probability of RDH and SDH Occurrences

Figure 2 presents the probability of rapidly and slowly evolving dry extremes followed by hot extremes (RDH and SDH) during 1980–2020, representing the fraction of dry extremes followed by hot extremes. Generally, both rapidly and slowly evolving dry extremes are likely to be followed by hot extremes, but the global distribution varies. The probabilities of RDH and SDH exhibit certain spatial similarities outside the northern mid-high latitudes (60°S–30°N) over time, such as in South America and Africa (Figure 2). However, there are disparities in the probabilities of RDH and SDH in the northern mid-high latitudes (≥30°N). Compared with slowly evolving dry extremes, rapidly evolving dry extremes are more likely to be followed by hot extremes in Western North America, Central North America, North Asia, Northern Europe, and East Asia (Figure 2), even across the two reanalysis data sets. Apart from the probability of RDH and SDH, the frequency of RDH occurrences in the northern mid-high latitudes is also higher than that of SDH (Figures 3a and 3c). We also examined the interannual changes in the global-averaged frequency of RDH and SDH, estimated as the mean value of grid cells that experienced RDH and SDH during the period of 1980–2020. Specifically, there is a more significant increase in the frequency of RDH compared to SDH globally during the recent period of 1980–2020 (Figures 3b and 3d), despite using different reanalysis data sets (Figure S2 in Supporting Information S1).

We further investigated the statistically significant changes in the distribution and shift in the median value of the probability of RDH and SDH using the two-sample Kolmogorov-Smirnov test (Figures 4a and 4c). The probability of hot extremes occurring after rapidly evolving dry extremes (43.22%−44.90%) shows a significant positive shift (at a 95% confidence level) in the median value compared to those after slowly evolving dry extremes (31.99%−32.78%). A higher probability of RDH compared to SDH is also identified when varying the thresholds used to detect the dry extremes (Figure S3 in Supporting Information S1). Notably, large disparities in the probability of RDH and SDH are also identified in the northern mid-high latitudes (Figures 4b and 4d). Quantitatively, the probability of hot extremes following rapidly evolving dry extremes is nearly twice as high as those following slowly evolving dry extremes in the northern mid-high latitudes. However, outside the northern

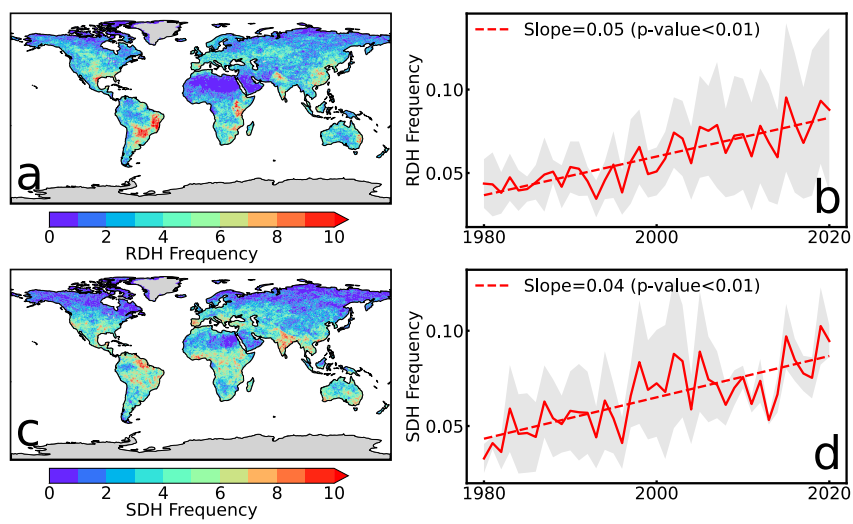

Figure 3. Spatiotemporal pattern of the total number of RDH and SDH during the period of 1980–2020. (a, c) Spatial pattern of the total number of RDH and SDH for each pixel during the period of 1980–2020 based on ERA5 and MERRA-2. (b, d) Annual time series (solid lines) of globally averaged RDH and SDH during the period of 1980–2020 based on the ensemble mean of ERA5 and MERRA-2. The linear annual trends (dashed lines) are estimated based on the Sen's slope estimator, and statistical significances in trends are determined based on the MK test for 1980–2020.

23284277, 2025, 5, Downloaded from https://agupubs.onlinelibrary.wiley.com/doi/10.1029/2024EF005151 by HONG KONG POLYTECHNIC UNIVERSITY HU NG HOM, Wiley Online Library on [29/09/2025]. See the Terms and Conditions (https://onlinelibrary.wiley.com/terms-and-conditions) on Wiley Online Library for rules of use; OA articles are governed by the applicable Creative Commons License

10.1029/2024EF005151

23284277, 2025, 5, Downloaded from https://agupubs.onlinelibrary.wiley.com/doi/10.1029/2024EF005151 by HONG KONG POLYTECHNIC UNIVERSITY HU NG HOM, Wiley Online Library on [29/09/2025]. See the Terms and Conditions (https://onlinelibrary.wiley.com/terms-and-conditions) on Wiley Online Library for rules of use; OA articles are governed by the applicable Creative Commons License

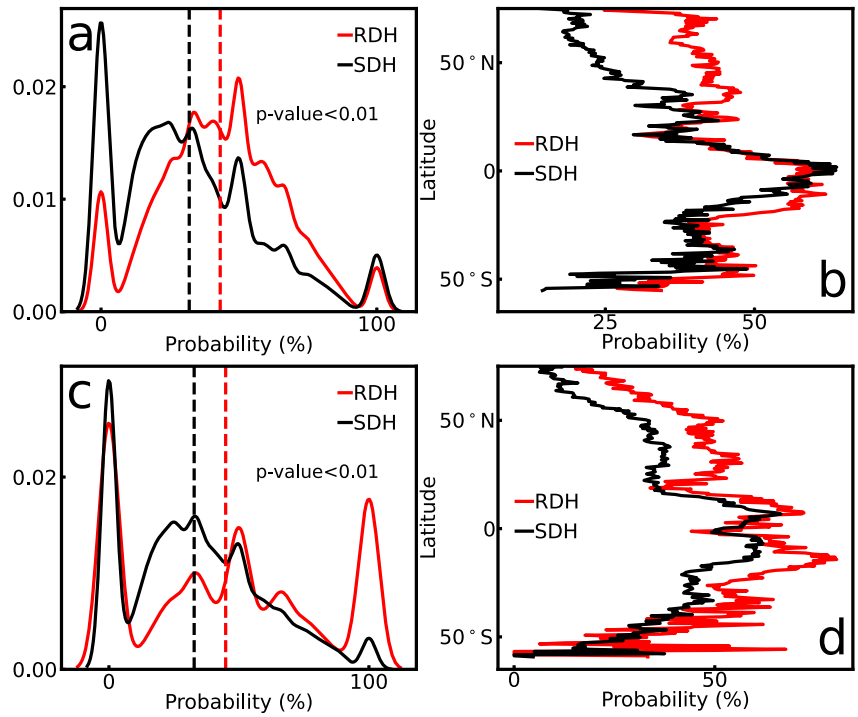

Figure 4. Comparison of probability of RDH and SDH globally. (a, c) Probability density functions of RDH and SDH based on the ERA5 and MERRA-2 data sets. (b, d) Line plots showing the latitudinal variation in the probability of RDH and SDH based on the ERA5 and MERRA-2 data sets.

mid-high latitudes, the probabilities of RDH and SDH are not significantly different. Therefore, while a dependence between dry extremes and hot extremes is expected, a stronger link has been identified between rapid soil dryness and hot extremes in the northern mid-high latitudes.

In addition to examining the effect of rapid soil dryness on subsequent hot extremes, we also compared how soil dryness recovery influences the development of hot events (Figure 5). Generally, there are no significant spatial disparities in the probability of RDH_R (hot extremes that prolong and recur following rapid soil dryness recovery) and SDH_R (hot extremes that prolong and recur following slow soil dryness recovery) on a global scale. However, the probability of SDH_R is higher than that of RDH_R. This suggests that, compared to quick soil moisture recovery, slower soil moisture recovery can prolong hot extremes or lead to recurring extremes. Therefore, the impact of rapid soil dryness on hot extremes is more pronounced during the onset of dryness, where quicker dryness occurrences are more likely to be accompanied by the development of hot extremes, potentially leading to cascading disasters.

3.2. Dynamic Response of Atmospheric Factors to RDH and SDH

Figure 6 shows the difference between soil moisture (SM) and maximum temperature (T_{max}) during RDH and SDH events. The SM during RDH is higher than during SDH, especially outside the northern mid-high latitudes, but it exhibits a larger anomaly compared to the climatological mean (Figure 6 and Figure S4 in Supporting Information S1). Although the difference in SM during RDH and SDH in the northern mid-high latitudes is relatively smaller compared to that outside these latitudes, the corresponding difference in T_{max} is indeed large. The T_{max} during RDH is more than 10°C higher than that during SDH in the northern mid-high latitudes, whereas the T_{max} during RDH and SDH is nearly similar outside these latitudes (Figure 6b). Rapidly evolving dry extremes (RD) is characterized by a rapid decrease in SM from the start (t-5 pentad) to dry conditions (t pentad) and continually maintaining dry conditions for at least three pentads (from t to $t + 2$ pentad). In contrast, changes in SM during slowly evolving dry extremes (SD) occur relatively gradually before reaching dry conditions in the t pentad. Meanwhile, the rapidly declining SM corresponds to a rapid rise in T_{max}. Specifically, the increase in T_{max}

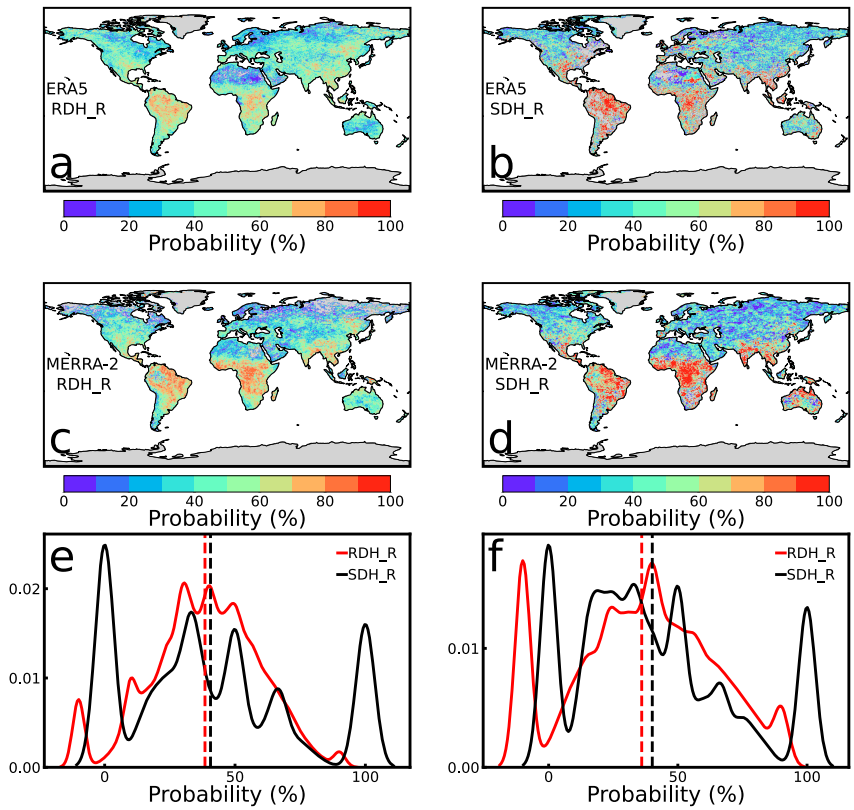

Figure 5. Comparison between the probabilities of RDH_R and SDH_R. (a, c) Spatial pattern of the probability of RDH_R during the period of 1980–2020 based on the ERA5 and MERRA-2 data sets. (b, d) Spatial pattern of the probability of SDH_R during the period of 1980–2020 based on the ERA5 and MERRA-2 data sets. (e, f) Probability density functions of RDH_R and SDH_R based on the ERA5 and MERRA-2 data sets.

from *t*-5 to *t* pentad during RD is about 4°C and 3°C for ERA5 and MERRA-2, respectively, which is much higher than that during SD for ERA5 (1°C) and MERRA-2 (1°C) (Figure 6).

We compared the mean variations in VPD, Rn, and Pre during RDH and SDH events (Figure 7). We find that a decrease in SM significantly increases VPD and Rn, and decreases Pre, indicating the negative sensitivities of VPD, and Rn, and the positive sensitivity of Pre to the SM decline as soils become drier, both during RDH and SDH. In comparison, VPD, Rn, and Pre during RDH experience larger changes. Specifically, the VPD, Rn, and Pre during RDH increase to 0.24−0.32 kPa, 0.73−0.95 10^5 J/m^2, and −2.70−−1.95 mm/day, whereas the VPD, Rn, and Pre during SDH only increase to 0.17−0.18 kPa, 0.18−0.32 10^5 J/m^2, and −1.7−−1.1 mm/day based on ERA5 and MERRA-2 (Figure 7). Furthermore, greater differences in VPD, Rn, and Pre between RDH and SDH were identified in the northern mid-to-high latitudes, indicating that the occurrence of RDH is consistently accompanied by increased atmospheric aridity (i.e., significantly higher VPD and lower Pre) and enhanced Rn compared to SDH in these latitudes (Figure 8). This pattern is consistent across both data sets (Figures S5 and S6 in Supporting Information S1).

The distinct atmospheric and environmental conditions associated with rapidly evolving dryness contribute to a higher likelihood of subsequent hot extremes compared to slowly evolving dryness, especially in the northern mid-high latitudes. Although both rapidly and slowly evolving dryness are characterized by elevated VPD and increased Rn, coupled with reduced Pre, rapidly evolving dryness exhibits larger positive anomalies in VPD and Rn, and more pronounced negative anomalies in Pre. These factors collectively create an environment conducive to rapid soil moisture depletion and heightened atmospheric demand for water. This rapid depletion of soil moisture reduces the land's ability to cool through evapotranspiration, leading to higher surface temperatures (Lian et al., 2021; Vereecken et al., 2022). Consequently, the combination of these factors results in a greater propensity for hot extremes to follow rapidly evolving dryness, as the land surface heats up more quickly and

23284277, 2025, 5, Downloaded from https://agupubs.onlinelibrary.wiley.com/doi/10.1029/2024EF005151 by HONG KONG POLYTECHNIC UNIVERSITY HU NG HOM, Wiley Online Library on [29/09/2025]. See the Terms and Conditions (https://onlinelibrary.wiley.com/terms-and-conditions) on Wiley Online Library for rules of use; OA articles are governed by the applicable Creative Commons License

10.1029/2024EF005151

23284277, 2025, 5, Downloaded from https://agupubs.onlinelibrary.wiley.com/doi/10.1029/2024EF005151 by HONG KONG POLYTECHNIC UNIVERSITY HU NG HOM, Wiley Online Library on [29/09/2025]. See the Terms and Conditions (https://onlinelibrary.wiley.com/terms-and-conditions) on Wiley Online Library for rules of use; OA articles are governed by the applicable Creative Commons License

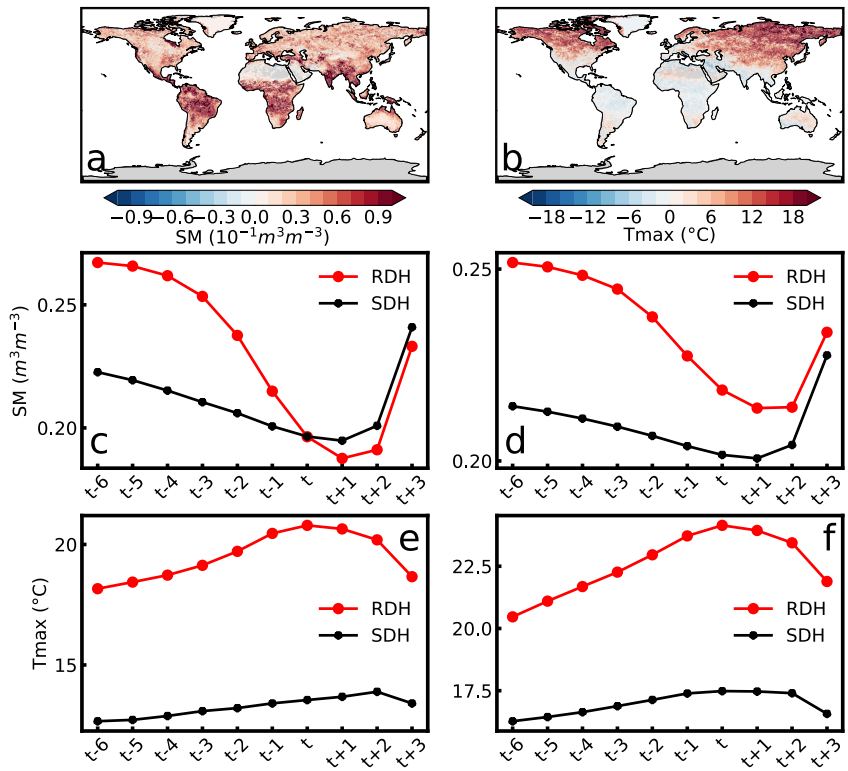

Figure 6. Dynamic response of SM and T_{max} to occurrence of RDH and SDH. (a, b) Spatial pattern of the difference in SM and T_{max} during the occurrence of RDH and SDH based on the ensemble mean of ERA5 and MERRA-2 data sets. (c, d) Temporal variation in SM during RDH and SDH for all grid points based on the ERA5 and MERRA-2 data sets. (e, f) Temporal variation in T_{max} during RDH and SDH for all grid points based on the ERA5 and MERRA-2 data sets.

intensely compared to the more gradual progression observed in slowly evolving dryness. This underscores the critical need for targeted monitoring and adaptive management strategies to mitigate the impacts of rapidly evolving dryness and their associated heat extremes.

3.3. Contribution of Soil Moisture–Atmosphere Couplings to the Occurrence of RDH and SDH

Soil moisture−atmosphere couplings have been suggested as an important mechanism to explain the evolution of dry and hot extremes, especially for dynamically connected extremes (Gallego-Elvira et al., 2016; Maraun et al., 2025; Vicente-Serrano et al., 2014). To investigate the role of VPD, Rn, and Pre in the interaction between SM and T_{max}, we sorted SM, VPD, Rn, and Pre into 10×10 bins and assessed the joint influence of SM and VPD, Rn, and Pre on T_{max} in each bin (Figure 9). We find that T_{max} is enhanced as VPD and Rn rise and Pre decreases under low SM conditions for both ERA5 and MERRA-2. For example, when SM is low (SM $\leq$ 10th percentile), a further increase in VPD and Rn, and a decrease in Pre correspond to a dramatic increase in T_{max}. The maximum T_{max} in the top-right bin in Figure 9 suggests that VPD, Rn, and Pre are important drivers of increased T_{max} after soil dryness. Additionally, higher VPD, and Rn and lower Pre correspond to a higher soil drying rate in the northern mid-high latitudes, showing a significant linear correlation between soil drying rate and atmospheric factors (i.e., VPD, Rn, and Pre) (Figure 10). This pattern is consistent across both data sets (Figure S7 in Supporting Information S1). However, outside the northern mid-high latitudes, VPD, Rn, and Pre do not show a significant increase or decrease with an increasing soil drying rate. These results suggest that T_{max} has a tighter dependence on the soil drying rate, accompanied by significant changes in VPD, Rn, and Pre. A higher T_{max} tends to follow a higher soil drying rate, causing a higher probability of hot extremes occurring after rapidly evolving dry extremes than after slowly evolving dry extremes in the northern mid-high latitudes.

To further explore the influence of soil moisture−atmosphere couplings on the occurrence of RDH and SDH, we investigated the role of SM−T_{max} coupling in the occurrence of these extremes using a probability multiplication

10.1029/2024EF005151

23284277, 2025, 5, Downloaded from https://agupubs.onlinelibrary.wiley.com/doi/10.1029/2024EF005151 by HONG KONG POLYTECHNIC UNIVERSITY HU NG HOM, Wiley Online Library on [29/09/2025]. See the Terms and Conditions (https://onlinelibrary.wiley.com/terms-and-conditions) on Wiley Online Library for rules of use; OA articles are governed by the applicable Creative Commons License

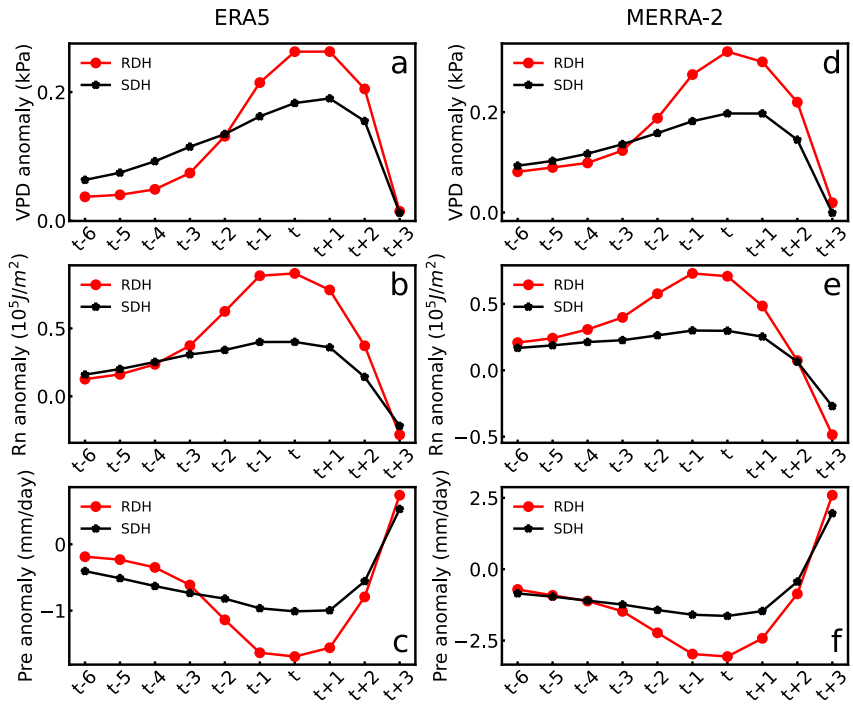

Figure 7. Dynamic response of atmospheric factors to occurrence of RDH and SDH. (a, d) Temporal variation in VPD anomalies during RDH and SDH for all grid points based on the ERA5 and MERRA-2 data sets. (b, e) Same as (a, d) but for Rn anomalies. (c, f) Same as (a, d) but for Pre anomalies.

factor (PMF). The PMF assesses the increase in the joint probability of occurrence of dry and subsequent hot extremes, compared to the probability expected if dry and hot extremes were independent. The joint probability of occurrence of dry and hot extremes is defined as the sequential occurrence of dry and hot extremes when SM is below its 10th percentile and the following T_{max} is above its 90th percentile. Higher PMF values (PMF > 1) indicate a higher probability of combined low SM and subsequent high T_{max} than expected if SM and T_{max} were uncoupled (Figures 11a and 11b). We find that there is a higher probability of RDH than SDH, even under the same strength of SM−T_{max} coupling. Furthermore, regions with stronger SM−T_{max} coupling witness a higher probability of RDH, which then reaches a steady state when the strength of SM−T_{max} coupling is extremely high. For example, regions without SM−T_{max} coupling (PMF ≤ 1) witness the lowest probability of RDH, which is significantly lower than that in regions with stronger SM−T_{max} coupling (PMF > 1). On the other hand, vegetation, land use, and soil types in different regions can alter SM−T_{max} coupling strength. Regions with sparse vegetation, such as bare areas and semi-arid regions, tend to experience stronger land−atmosphere coupling, whereas densely vegetated areas like forests may exhibit weaker coupling, as abundant vegetation moderates the exchange of heat and moisture between the land and the atmosphere (Figures 11c and 11d). The evident differences in SM−T_{max} coupling strength across various land cover categories suggest that changes in land cover will also affect land−atmosphere coupling, thereby influencing the occurrence of RDH and SDH.

Admittedly, extreme events, including dry and hot extremes, are associated with large−scale atmospheric circulation patterns (AghaKouchak et al., 2020; Alizadeh et al., 2020). Apart from the large−scale atmospheric circulation, the role of land−atmosphere coupling cannot be ignored. A dry extreme event triggered by persistent large−scale circulation anomalies would further induce a subsequent hot extreme, forming cascading dry and hot extreme events under the influence of land−atmosphere coupling. For example, a modeling study of the 2010 Russian heatwave (Hauser et al., 2016) identified a 13-fold increase in the probability of exceeding the previous summer heat record due to soil moisture deficits, whereas sea surface temperature anomalies in 2010 did not have a strong impact on the occurrence of the event. As soils dry out under land−atmosphere interactions, evaporation progressively declines, and a larger proportion of incoming radiation can lead to an accumulation of sensible heat in the atmosphere, potentially developing into a heatwave or exaggerating its magnitude. Moreover, due to land−atmosphere couplings, more intense warming is likely to follow more rapidly evolving dry extremes, such

10.1029/2024EF005151

23284277, 2025, 5, Downloaded from https://agupubs.onlinelibrary.wiley.com/doi/10.1029/2024EF005151 by HONG KONG POLYTECHNIC UNIVERSITY HU NG HOM, Wiley Online Library on [29/09/2025]. See the Terms and Conditions (https://onlinelibrary.wiley.com/terms-and-conditions) on Wiley Online Library for rules of use; OA articles are governed by the applicable Creative Commons License

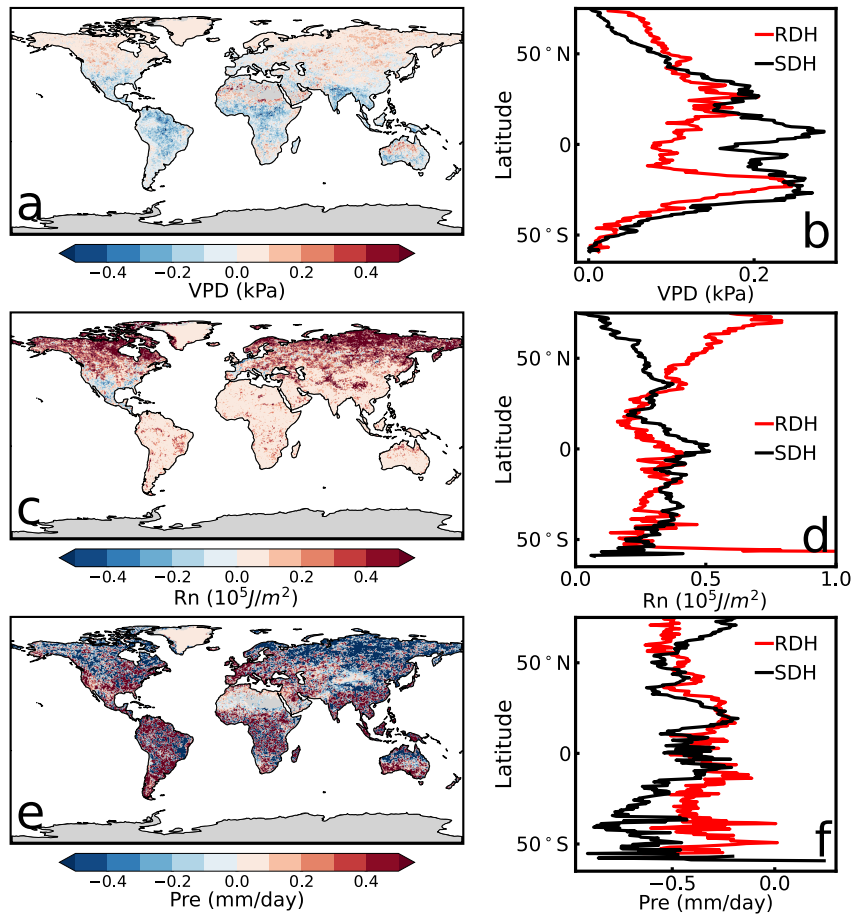

Figure 8. Difference between atmospheric factors during the occurrence of RDH and SDH. (a) Spatial pattern of the difference in VPD during the occurrence of RDH and SDH based on the ensemble mean of ERA5 and MERRA-2 data sets. (b) Line plots showing the latitudinal variation in the VPD during RDH and SDH based on the ensemble mean of ERA5 and MERRA-2 data sets. (c, d) Same as (a, b) but for Rn. (e, f) Same as (a, b) but for Pre.

as the occurrence of flash droughts followed by heatwaves observed in Russia (Christian et al., 2020) and the central U.S. in 2012 (Otkin et al., 2016).

4. Conclusions and Discussions

We conducted a sensitivity analysis by changing the depths of SM. Compared with deep SM, SM in shallow soil layers responds faster to meteorological anomalies and interacts more closely with the atmosphere and its evaporative demand (Li & Huang, 2021; Wang et al., 2021). By comparing the probabilities of occurrence of rapidly and slowly evolving dry and hot extremes using root-zone SM, we find a similar pattern of the probabilities of RDH and SDH across different soil depths. In comparison, the probability of RDH based on root-zone SM is smaller than that based on surface SM (Figure S8 in Supporting Information S1).

In this work, we focused on the local processes of the evolution of dry and hot extremes. However, limiting our analysis to the same location may overlook the broader impact of tele-connected processes. In fact, dry and hot extremes are not only shaped by local conditions but can also be influenced by remote soil moisture deficits through atmospheric processes. For instance, as upwind dryness (source) occurs, the reduction in evaporation results in less moisture being transported to downwind locations, causing the air to become drier. This evaporation deficit allows a larger proportion of incoming radiation to accumulate as sensible heat in the atmosphere, potentially intensifying hot extremes in downwind regions (Schumacher et al., 2019, 2022). The transport of water vapor across the

10.1029/2024EF005151

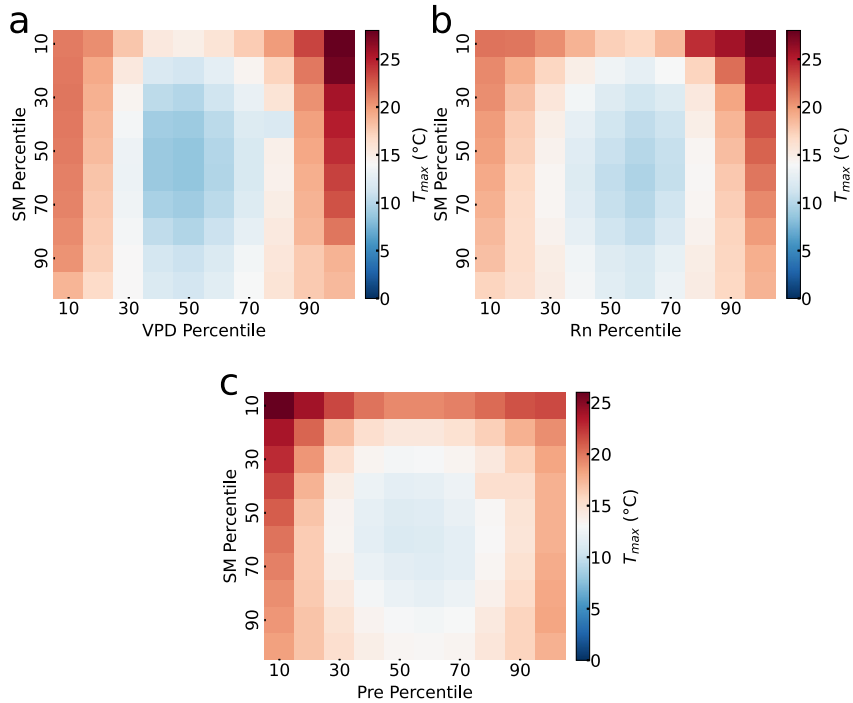

Figure 9. Relationships among SM, VPD, Rn, Pre, and T_{max}. (a) Joint influence of SM and VPD on the T_{max} in each percentile bin based on the ensemble of ERA5 and MERRA-2 data sets. (b) Joint influence of SM and Rn on the T_{max} in each percentile bin based on the ensemble of ERA5 and MERRA-2 data sets. (c) Joint influence of SM and Pre on the T_{max} in each percentile bin based on the ensemble of ERA5 and MERRA-2 data sets.

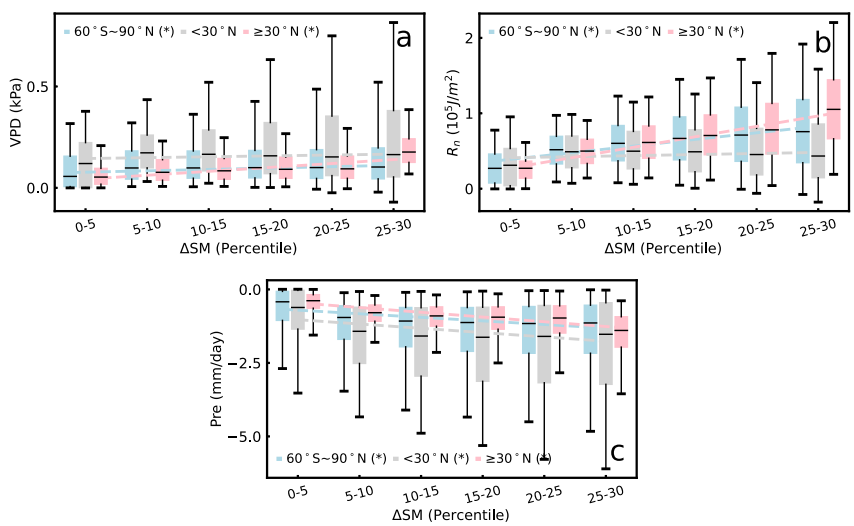

Figure 10. Relationships between atmospheric factors and soil drying rate. (a) Box plots of different soil drying rates and the corresponding VPD globally, outside the northern mid-high latitudes (60°S−30°N), and in the northern mid-high latitudes (≥30°N) based on the ensemble of ERA5 and MERRA-2 data sets. The short horizontal line inside the box represents the 50th percentile, and the top and bottom of the box represent the 75th and 25th percentiles, respectively. The top and bottom of the line represent the 95th and 5th percentiles, respectively. The linear annual trends (dashed lines) are estimated based on the Sen's slope estimator, and statistical significances in trends are determined based on the MK test. (b and c) Same as (a) but for Rn and Pre.

23284277, 2025, 5, Downloaded from https://agupubs.onlinelibrary.wiley.com/doi/10.1029/2024EF005151 by HONG KONG POLYTECHNIC UNIVERSITY HU NG HOM, Wiley Online Library on [29/09/2025]. See the Terms and Conditions (https://onlinelibrary.wiley.com/terms-and-conditions) on Wiley Online Library for rules of use; OA articles are governed by the applicable Creative Commons License

10.1029/2024EF005151

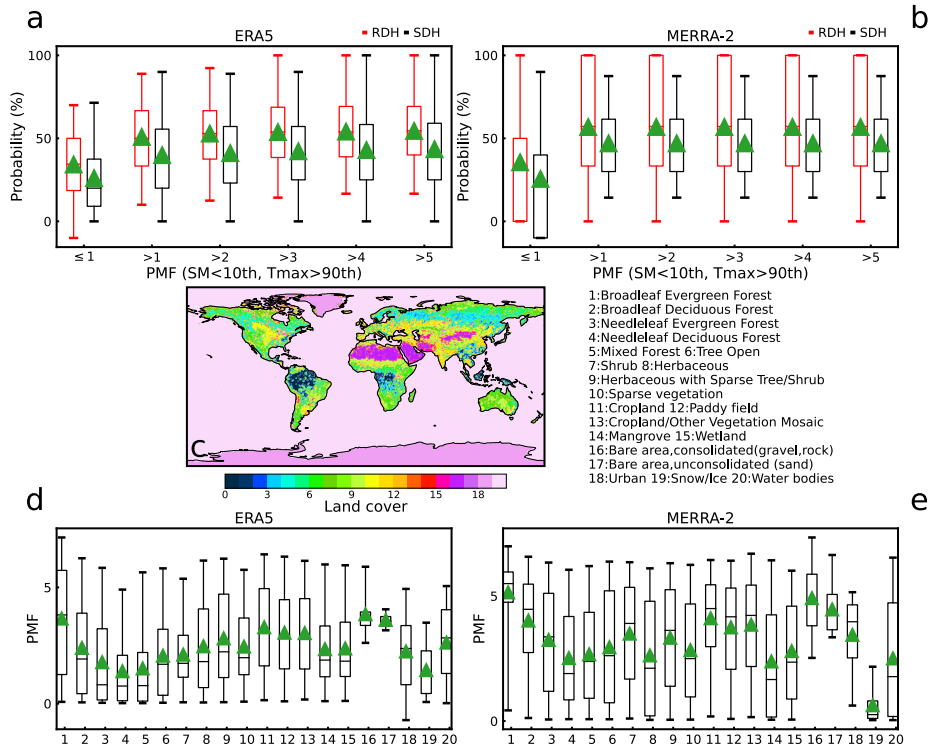

Figure 11. Contribution of SM−T_{max} coupling to the occurrence of RDH and SDH. (a) Bar plots of the probability of RDH and SDH that occur in regions with different SM−T_{max} coupling strengths (i.e., PMF ≤ 1, PMF > 1, PMF > 2, PMF > 3, PMF > 4, and PMF > 5) based on ERA5. (b) Bar plots of the probability of RDH and SDH that occur in regions with different SM−T_{max} coupling strengths (i.e., PMF ≤ 1, PMF > 1, PMF > 2, PMF > 3, PMF > 4, and PMF > 5) based on MERRA-2. (c) Map of land cover (GLCNMO) with 20 categories. (d, e) Bar plots of the SM−T_{max} coupling strengths (i.e., PMF values) across different categories of land cover based on ERA5 and MERRA-2 data sets.

continent facilitates these remote linkages (Herrera-Estrada et al., 2019; Keune et al., 2022; Liu et al., 2021), which can partly explain the occurrence of hot extremes following soil drying in distant areas. Therefore, while our study focuses on local interactions, tele-connected compound dry and hot extremes are also critical and warrant further investigation.

Our study identifies the global hotspots of cascading dry and hot extremes and the dependence between dry extreme outbreaks and subsequent hot extremes: soil drying can activate the soil moisture−atmosphere interactions necessary to elevate surface temperatures, leading to hot extremes. Particularly, the more intensified SM decline during the onset phase of dry extremes is likely to induce more hot extremes. The initial SM condition during the onset phase of dry extremes, especially the soil drying rate, can be viewed as a possible precursor for the occurrence of hot extremes. The identification of global hotspots and the underlying mechanisms of rapidly evolving dry-hot extremes facilitates the assessment of potential risks to crop yields, wildfires, and water scarcity across the globe.

Conflict of Interest

The authors declare no conflicts of interest relevant to this study.

Data Availability Statement

The gridded hourly soil moisture, 2 m temperature, 2 m dewpoint temperature, precipitation, and surface net solar radiation can be accessible from (a) the ERA5 (Hersbach et al., 2023a, 2023b) and (b) the MERRA-2 (Gelaro et al., 2017).

23284277, 2025, 5, Downloaded from https://agupubs.onlinelibrary.wiley.com/doi/10.1029/2024EF005151 by HONG KONG POLYTECHNIC UNIVERSITY HU NG HOM, Wiley Online Library on [29/09/2025]. See the Terms and Conditions (https://onlinelibrary.wiley.com/terms-and-conditions) on Wiley Online Library for rules of use; OA articles are governed by the applicable Creative Commons License

Acknowledgments
The work described in this paper was partially supported by a grant from the Research Grants Council of the Hong Kong Special Administrative Region, China (Project No. PolyU/RGC 15232023) and the Hong Kong Polytechnic University (Project No. P0045957, P0043040).

References

AghaKouchak, A., Cheng, L., Mazdiyasni, O., & Farahmand, A. (2014). Global warming and changes in risk of concurrent climate extremes: Insights from the 2014 California drought. *Geophysical Research Letters*, *41*(24), 8847–8852. https://doi.org/10.1002/2014GL062308

AghaKouchak, A., Chiang, F., Huning, L. S., Love, C. A., Mallakpour, I., Mazdiyasni, O., et al. (2020). Climate extremes and compound hazards in a warming world. *Annual Review of Earth and Planetary Sciences*, *48*(1), 519–548. https://doi.org/10.1146/annurev-earth-071719-055228

Alizadeh, M. R., Adamowski, J., Nikoo, M. R., AghaKouchak, A., Dennison, P., & Sadegh, M. (2020). A century of observations reveals increasing likelihood of continental-scale compound dry-hot extremes. *Science Advances*, *6*(39), eaaz4571. https://doi.org/10.1126/sciadv.aaz457

Bevacqua, E., Zappa, G., Lehner, F., & Zscheischler, J. (2022). Precipitation trends determine future occurrences of compound hot–dry events. *Nature Climate Change*, *12*(4), 350–355. https://doi.org/10.1038/s41558-022-01309-5

Chiang, F., Mazdiyasni, O., & AghaKouchak, A. (2018). Amplified warming of droughts in southern United States in observations and model simulations. *Science Advances*, *4*(8), eaat2380. https://doi.org/10.1126/sciadv.aat2380

Christian, J. I., Basara, J. B., Hunt, E. D., Otkin, J. A., & Xiao, X. (2020). Flash drought development and cascading impacts associated with the 2010 Russian heatwave. *Environmental Research Letters*, *15*(9), 094078. https://doi.org/10.1088/1748-9326/ab9faf

European Environment Agency. (2023). *Economic losses from climate-related extremes in Europe* [WWW Document]. European Environment Agency. Retrieved from https://www.eea.europa.eu/data-and-maps/indicators/direct-losses-from-weather-disasters-3/assessment-2

Feng, S., Wu, X., Hao, Z., Hao, Y., Zhang, X., & Hao, F. (2020). A database for characteristics and variations of global compound dry and hot events. *Weather and Climate Extremes*, *30*, 100299. https://doi.org/10.1016/j.wace.2020.100299

Fischer, E. M., & Schär, C. (2010). Consistent geographical patterns of changes in high-impact European heatwaves. *Nature Geoscience*, *3*(6), 398–403. https://doi.org/10.1038/ngeo866

Fischer, E. M., Seneviratne, S. I., Vidale, P. L., Lüthi, D., & Schär, C. (2007). Soil moisture–atmosphere interactions during the 2003 European summer heat wave. *Journal of Climate*, *20*(20), 5081–5099. https://doi.org/10.1175/JCLI4288.1

Ford, T. W., & Labosier, C. F. (2017). Meteorological conditions associated with the onset of flash drought in the Eastern United States. *Agricultural and Forest Meteorology*, *247*, 414–423. https://doi.org/10.1016/j.agrformet.2017.08.031

Gallego-Elvira, B., Taylor, C. M., Harris, P. P., Ghent, D., Veal, K. L., & Folwell, S. S. (2016). Global observational diagnosis of soil moisture control on the land surface energy balance. *Geophysical Research Letters*, *43*(6), 2623–2631. https://doi.org/10.1002/2016GL068178

Gelaro, R., McCarty, W., Suárez, M. J., Todling, R., Molod, A., Takacs, L., et al. (2017). The modern-era retrospective analysis for research and applications, version 2 (MERRA-2) [Dataset]. *Journal of Climate*, *30*(14), 5419–5454. https://doi.org/10.1175/JCLI-D-16-0758.1

Graham, D. J., Bierkens, M. F., & van Vliet, M. T. (2024). Impacts of droughts and heatwaves on river water quality worldwide. *Journal of Hydrology*, *629*, 130590. https://doi.org/10.1016/j.jhydrol.2023.130590

Hao, Z., Hao, F., Xia, Y., Feng, S., Sun, C., Zhang, X., et al. (2022). Compound droughts and hot extremes: Characteristics, drivers, changes, and impacts. *Earth-Science Reviews*, *235*, 104241. https://doi.org/10.1016/j.earscirev.2022.104241

Hauser, M., Orth, R., & Seneviratne, S. I. (2016). Role of soil moisture versus recent climate change for the 2010 heat wave in western Russia. *Geophysical Research Letters*, *43*(6), 2819–2826. https://doi.org/10.1002/2016GL068036

Herrera-Estrada, J. E., Martinez, J. A., Dominguez, F., Findell, K. L., Wood, E. F., & Sheffield, J. (2019). Reduced moisture transport linked to drought propagation across North America. *Geophysical Research Letters*, *46*(10), 5243–5253. https://doi.org/10.1029/2019GL082475

Hersbach, H., Bell, B., Berrisford, P., Hirahara, S., Horányi, A., Muñoz-Sabater, J., et al. (2023a). ERA5 monthly averaged data on single levels from 1940 to present [Dataset]. *Copernicus Climate Change Service (C3S) Climate Data Store (CDS)*. https://doi.org/10.24381/cds.f17050d7

Hersbach, H., Bell, B., Berrisford, P., Hirahara, S., Horányi, A., Muñoz-Sabater, J., et al. (2023b). ERA5 monthly averaged data on pressure levels from 1940 to present [Dataset]. *Copernicus Climate Change Service (C3S) Climate Data Store (CDS)*. https://doi.org/10.24381/cds.6860a573

Kang, Y., Guo, E., Wang, Y., Bao, Y., Bao, Y., Mandula, N., et al. (2022). Characterisation of compound dry and hot events in Inner Mongolia and their relationship with large-scale circulation patterns. *Journal of Hydrology*, *612*, 128296. https://doi.org/10.1016/j.jhydrol.2022.128296

Keune, J., Schumacher, D. L., Dirmeyer, P., & Miralles, D. G. (2022). Drought self-propagation in drylands through moisture recycling. In *EGU General Assembly Conference Abstracts* (pp. EGU22–9139).

Kolmogorov, A. N. (1933). *Sulla determinazione empirica di una legge didistribuzione* (Vol. 4, pp. 83–91). Giornale dell'Istituto Italiano degli Attuari.

Li, X., & Huang, W. R. (2021). How long should the pre-existing climatic water balance be considered when capturing short-term wetness and dryness over China by using SPEI? *Science of the Total Environment*, *786*, 147575. https://doi.org/10.1016/j.scitotenv.2021.147575

Lian, X., Piao, S., Chen, A., Huntingford, C., Fu, B., Li, L. Z. X., et al. (2021). Multifaceted characteristics of dryland aridity changes in a warming world. *Nature Reviews Earth and Environment*, *2*(4), 232–250. https://doi.org/10.1038/s43017-021-00144-0

Liberto, T. D. (2021). Record-breaking June 2021 heatwave impacts the U.S. West. NOAA Climate.gov. Retrieved from https://www.climate.gov/news-features/event-tracker/record-breaking-june-2021-heatwave-impacts-us-west

Liu, Y., Liu, Y., Wang, W., & Zhou, H. (2021). Propagation of soil moisture droughts in a hotspot region: Spatial pattern and temporal trajectory. *Journal of Hydrology*, *593*, 125906. https://doi.org/10.1016/j.jhydrol.2020.125906

Maraun, D., Schiemann, R., Ossó, A., & Jury, M. (2025). Changes in event soil moisture-temperature coupling can intensify very extreme heat beyond expectations. *Nature Communications*, *16*(1), 734. https://doi.org/10.1038/s41467-025-56109-0

Miralles, D. G., Schumacher, D., Keune, J., van Heerwaarden, C., de Arellano, J. V. G., Gentine, P., et al. (2019). Mega-heatwave temperatures driven by local and upwind soil desiccation. *Geophysical Research Abstracts*, *21*.

Miralles, D. G., Teuling, A. J., Van Heerwaarden, C. C., & Vilà-Guerau de Arellano, J. (2014). Mega-heatwave temperatures due to combined soil desiccation and atmospheric heat accumulation. *Nature Geoscience*, *7*(5), 345–349. https://doi.org/10.1038/ngeo2141

Mukherjee, S., Ashfaq, M., & Mishra, A. K. (2020). Compound drought and heatwaves at a global scale: The role of natural climate variability-associated synoptic patterns and land-surface energy budget anomalies. *Journal of Geophysical Research: Atmospheres*, *125*(11), e2019JD031943. https://doi.org/10.1029/2019JD031943

Mukherjee, S., & Mishra, A. K. (2021). Increase in compound drought and heatwaves in a warming world. *Geophysical Research Letters*, *48*(1), e2020GL090617. https://doi.org/10.1029/2020GL090617

Mukherjee, S., Mishra, A. K., Zscheischler, J., & Entekhabi, D. (2023). Interaction between dry and hot extremes at a global scale using a cascade modeling framework. *Nature Communications*, *14*(1), 277. https://doi.org/10.1038/s41467-022-35748-7

Osman, M., Zaitchik, B. F., & Winstead, N. S. (2022). Cascading drought-heat dynamics during the 2021 Southwest United States heatwave. *Geophysical Research Letters*, *49*(12), e2022GL099265. https://doi.org/10.1029/2022GL099265

23284277, 2025, 5, Downloaded from https://agupubs.onlinelibrary.wiley.com/doi/10.1029/2024EF005151 by HONG KONG POLYTECHNIC UNIVERSITY HU NG HOM, Wiley Online Library on [29/09/2025]. See the Terms and Conditions (https://onlinelibrary.wiley.com/terms-and-conditions) on Wiley Online Library for rules of use; OA articles are governed by the applicable Creative Commons License

Otkin, J. A., Anderson, M. C., Hain, C., Svoboda, M., Johnson, D., Mueller, R., et al. (2016). Assessing the evolution of soil moisture and vegetation conditions during the 2012 United States flash drought. *Agricultural and Forest Meteorology*, *218*, 230–242. https://doi.org/10.1016/j.agrformet.2015.12.065

Park Williams, A., Allen, C. D., Macalady, A. K., Griffin, D., Woodhouse, C. A., Meko, D. M., et al. (2013). Temperature as a potent driver of regional forest drought stress and tree mortality. *Nature Climate Change*, *3*(3), 292–297. https://doi.org/10.1038/nclimate1693

Perkins, S. E., & Alexander, L. V. (2013). On the measurement of heat waves. *Journal of Climate*, *26*, 4500–4517. https://doi.org/10.1029/2012GL053361

Qing, Y., Wang, S., Ancell, B. C., & Yang, Z. L. (2022). Accelerating flash droughts induced by the joint influence of soil moisture depletion and atmospheric aridity. *Nature Communications*, *13*(1), 1139. https://doi.org/10.1038/s41467-022-28752-4

Raymond, C., Horton, R. M., Zscheischler, J., Martius, O., AghaKouchak, A., Balch, J., et al. (2020). Understanding and managing connected extreme events. *Nature Climate Change*, *10*(7), 611–621. https://doi.org/10.1038/s41558-020-0790-4

Rippey, B. R. (2015). The US drought of 2012. *Weather and Climate Extremes*, *10*, 57–64. https://doi.org/10.1016/j.wace.2015.10.004

Robine, J. M., Cheung, S. L. K., Le Roy, S., Van Oyen, H., Griffiths, C., Michel, J. P., & Herrmann, F. R. (2008). Death toll exceeded 70,000 in Europe during the summer of 2003. *Comptes Rendus Biologies*, *331*(2), 171–178. https://doi.org/10.1016/j.crvi.2007.12.001

Schubert, S. D., Suarez, M. J., Pegion, P. J., Koster, R. D., & Bacmeister, J. T. (2004). On the cause of the 1930s dust bowl. *Science*, *303*(5665), 1855–1859. https://doi.org/10.1126/science.1095048

Schumacher, D. L., Keune, J., Dirmeyer, P., & Miralles, D. G. D. (2022). Drought self-propagation in drylands due to land–atmosphere feedbacks. *Nature Geoscience*, *15*(4), 262–268. https://doi.org/10.1038/s41561-022-00912-7

Schumacher, D. L., Keune, J., Van Heerwaarden, C. C., Vilà-Guerau de Arellano, J., Teuling, A. J., & Miralles, D. G. (2019). Amplification of mega-heatwaves through heat torrents fuelled by upwind drought. *Nature Geoscience*, *12*(9), 712–717. https://doi.org/10.1038/s41561-019-0431-6

Seneviratne, S. I., Zhang, X., Adnan, M., Badi, W., Dereczynski, C., Di Luca, A., et al. (2021). 11 Chapter 11: Weather and climate extreme events in a changing climate.

Seneviratne, S. I., Lüthi, D., Litschi, M., & Schär, C. (2006). Land–atmosphere coupling and climate change in Europe. *Nature*, *443*(7108), 205–209. https://doi.org/10.1038/nature05095

Tian, Y., Giaquinto, D., Di Capua, G., Claassen, J. N., Ali, J., Li, H., & De Michele, C. (2024). Historical changes in the Causal Effect Networks of compound hot and dry extremes in central Europe. *Communications Earth and Environment*, *5*(1), 1–14. https://doi.org/10.1038/s43247-024-01934-2

Tripathy, K. P., Mukherjee, S., Mishra, A. K., Mann, M. E., & Williams, A. P. (2023). Climate change will accelerate the high-end risk of compound drought and heatwave events. *Proceedings of the National Academy of Sciences of the United States of America*, *120*(28), e2219825120. https://doi.org/10.1073/pnas.2219825120

Vereecken, H., Amelung, W., Bauke, S. L., Bogena, H., Brüggemann, N., Montzka, C., et al. (2022). Soil hydrology in the Earth system. *Nature Reviews Earth and Environment*, *3*(9), 573–587. https://doi.org/10.1038/s43017-022-00324-6

Vicente-Serrano, S. M., Lopez-Moreno, J. I., Beguería, S., Lorenzo-Lacruz, J., Sanchez-Lorenzo, A., García-Ruiz, J. M., et al. (2014). Evidence of increasing drought severity caused by temperature rise in southern Europe. *Environmental Research Letters*, *9*(4), 044001. https://doi.org/10.1088/1748-9326/9/4/044001

Vogel, M. M., Orth, R., Cheruy, F., Hagemann, S., Lorenz, R., van den Hurk, B. J. J. M., & Seneviratne, S. I. (2017). Regional amplification of projected changes in extreme temperatures strongly controlled by soil moisture-temperature feedbacks. *Geophysical Research Letters*, *44*(3), 1511–1519. https://doi.org/10.1002/2016GL071235

Wang, J., DeFlorio, M. J., Gershunov, A., Guirguis, K., Delle Monache, L., & Ralph, F. M. (2024). Association of western US compound hydrometeorological extremes with Madden-Julian oscillation and ENSO interaction. *Communications Earth and Environment*, *5*(1), 314. https://doi.org/10.1038/s43247-024-01449-w

Wang, Y., Zhang, Y., Yu, X., Jia, G., Liu, Z., Sun, L., et al. (2021). Grassland soil moisture fluctuation and its relationship with evapotranspiration. *Ecological Indicators*, *131*, 108196. https://doi.org/10.1016/j.ecolind.2021.108196

Wu, X., Hao, Z., Hao, F., Zhang, X., Singh, V. P., & Sun, C. (2021). Influence of large-scale circulation patterns on compound dry and hot events in China. *Journal of Geophysical Research: Atmospheres*, *126*(4), e2020JD033918. https://doi.org/10.1029/2020JD033918

Yin, J., Gentine, P., Slater, L., Gu, L., Pokhrel, Y., Hanasaki, N., et al. (2023). Future socio-ecosystem productivity threatened by compound drought–heatwave events. *Nature Sustainability*, *6*(3), 259–272. https://doi.org/10.1038/s41893-022-01024-1

Yoon, J.-H., Kravitz, B., Rasch, P. J., Simon Wang, S.-Y., Gillies, R. R., & Hipps, L. (2015). Extreme fire season in California: A glimpse into the future? *Bulletin of the American Meteorological Society*, *96*(12), S5–S9. https://doi.org/10.1175/bams-d-15-00114.1

You, J., Wang, S., Zhang, B., Raymond, C., & Matthews, T. (2023). Growing threats from swings between hot and wet extremes in a warmer world. *Geophysical Research Letters*, *50*(14), e2023GL104075. https://doi.org/10.1029/2023GL104075

Yuan, X., Wang, Y., Ji, P., Wu, P., Sheffield, J., & Otkin, J. A. (2023). A global transition to flash droughts under climate change. *Science*, *380*(6641), 187–191. https://doi.org/10.1126/science.abn6301

Zeighami, A., Kern, J., Yates, A. J., Weber, P., & Bruno, A. A. (2023). US West Coast droughts and heat waves exacerbate pollution inequality and can evade emission control policies. *Nature Communications*, *14*(1), 1415. https://doi.org/10.1038/s41467-023-37080-0

Zhang, Y., Hao, Z., Feng, S., Zhang, X., & Hao, F. (2022). Changes and driving factors of compound agricultural droughts and hot events in eastern China. *Agricultural Water Management*, *263*, 107485. https://doi.org/10.1016/j.agwat.2022.107485

Zhou, S., Williams, A. P., Lintner, B. R., Berg, A. M., Zhang, Y., Keenan, T. F., et al. (2021). Soil moisture–atmosphere feedbacks mitigate declining water availability in drylands. *Nature Climate Change*, *11*(1), 38–44. https://doi.org/10.1038/s41558-020-00945-z

Zscheischler, J., & Seneviratne, S. I. (2017). Dependence of drivers affects risks associated with compound events. *Science Advances*, *3*(6), e1700263. https://doi.org/10.1126/sciadv.170026

23284277, 2025, 5, Downloaded from https://agupubs.onlinelibrary.wiley.com/doi/10.1029/2024EF005151 by HONG KONG POLYTECHNIC UNIVERSITY HU NG HOM, Wiley Online Library on [29/09/2025]. See the Terms and Conditions (https://onlinelibrary.wiley.com/terms-and-conditions) on Wiley Online Library for rules of use; OA articles are governed by the applicable Creative Commons License